Nano Hybrids *Online: 2013-01-25*
ISSN: 2234-9871, Vol. 3, pp 1-23
doi:10.4028/www.scientific.net/NH.3.1

Electrokinetic and Impedimetric Dynamics of FeCo-Nanoparticles on Glassy Carbon Electrode

Chinwe O. Ikpo[a], Njagi Njomo[a], Kenneth I. Ozoemena[b], Tesfaye Waryo[a], Rasaq A. Olowu[a], Milua Masikini[a], Abd Almonam Baleg[a], Nazeem Jahed[a], Priscilla G. L. Baker[a], Emmanuel I. Iwuoha[a, *]

[a]SensorLab, Department of Chemistry, University of Western Cape, Moderddam Road, Bellville, Cape Town 7535, South Africa

[b]Energy and Processes Division, Materials Science and Manufacturing, Council for Scientific and Industrial Research (CSIR) Pretoria 0001, South Africa

*eiwuoha@uwc.ac.za (corresponding author)

Keywords: Chemically modified electrodes, $LiClO_4$ in ethylene carbonate-dimethyl carbonate, iron-cobalt nanoparticles, cyclic voltammetry, electrochemical impedance spectroscopy, diffusion coefficient, charge transfer resistance

Abstract. The electrochemical dynamics of a film of FeCo nanoparticles were studied on a glassy carbon electrode (GCE). The film was found to be electroactive in 1 M $LiClO_4$ containing 1:1 v/v ethylene carbonate – dimethyl carbonate electrolyte system. Cyclic voltammetric experiments revealed a diffusion-controlled electron transfer process on the GCE/FeCo electrode surface. Further interrogation on the electrochemical properties of the FeCo nanoelectrode in an oxygen saturated 1 M $LiClO_4$ containing 1:1 v/v ethylene-carbonate-dimethyl carbonate revealed that the nanoelectrode showed good response towards the electro-catalytic reduction of molecular oxygen with a Tafel slope of about 120 mV which is close to the theoretical 118 mV for a single electron transfer process in the rate limiting step; and a transfer coefficient (α) of 0.49. The heterogeneous rate constant of

electron transfer (k_{et}), exchange current density (i_o) and time constant (τ) were calculated from data obtained from electrochemical impedance spectroscopy and found to have values of 2.3 x 10^{-5} cm s^{-1}, 1.6 x 10^{-4} A cm^{-2} and 2.4 x 10^{-4} s rad^{-1}, respectively.

Introduction

Modifying the surface of an electrode to provide some control over how the electrode interacts with its environment is one of the most active areas of research in electrochemistry [1]. The ability to chemically modify electrodes has provided a powerful route to tuning their performance. This has been of particular importance for research into energy storage devices [2], corrosion protection [3], molecular electronics [4], electrochromic devices [5], electrochemical sensing and fundamental research into phenomena that influence electrochemical processes. The distinguishing feature of a chemically modified electrode is that a thin film of a selected chemical is bonded or coated onto the electrode surface to endow the electrode with unique electronic, optical, and catalytic properties [6].

Glassy carbon electrodes are commonly employed in electrochemical applications due to their excellent properties which include low background currents, wide potential window, low electrical resistance and a reproducible surface structure that can be easily cleaned. They show wide thermal stability and morphological diversity [7-8]. The surface of a GCE can be modified in a number of ways in order to improve its performance in various electrochemical systems. Conducting polymers [9-10], carbon nanotubes [11], nanoparticles [12-14] have all been used to modify glassy carbon surfaces. In recent years, modification of solid electrodes with nanoparticles has attracted considerable interest. Unlike bulk films, metal nanoparticles exhibit unusual property of quantized double layer charging effects. The main advantages to the use of nanoparticles modified electrode are high effective surface area and enhanced electron transfer rate [15] which constitute a part of the driving force in developing nanosized electrocatalysts. However, bimetallic nanoparticles are proved to have superior catalytic properties than pure metals due to the electronic interactions that occur

between the components of the bimetallic system [16-17]. Bimetallic FeCo nanoparticles in particular, are receiving wide attention in view of their potential scientific and technological applications.

FeCo nanoparticles are important soft magnetic materials with a variety of structural [18-20], electronic [21-22], mechanical [23-24], optical [21] and electro-catalytic properties [25]. A lot of research has been conducted in the past to synthesize and characterize FeCo nanoparticles and their composites [22, 26-30]. However, scanty literature exists on their electrochemical behaviour on solid electrodes in $LiClO_4$ electrolytic solution containing 1:1 v/v ethylene carbonate-dimethyl carbonate (EC-DC) solvent mixture. Therefore, the electrochemical behaviour of a film of FeCo nanoparticles on a GCE in the above electrolyte is presented.

Experimental Section

Chemicals. Iron (II) sulfate heptahydrate ($FeSO_4.7H_2O$, Sigma), cobalt (II) chloride hexahydrate ($CoCl_2.6H_2O$, Sigma Aldrich), sodium borohydride ($NaBH_4$, 98%, Sigma Aldrich), triethylamine ($C_6H_{15}N$, 99.5%, Sigma Aldrich), ethanol (C_2H_6O, absolute, Sigma Aldrich), acetone (C_3H_6O, 99.8 %, Sigma Aldrich), lithium perchlorate ($LiClO_4$, 99.99%, Sigma Aldrich), ethylene carbonate ($C_3H_4O_3$, 99 %, Sigma Aldrich) and dimethyl carbonate ($(CH_3O)_2CO$, 99%, Sigma Aldrich) were used as received. Water obtained from a Millipore Milli-Q purification system with resistivity 18.2 MΩ was used to prepare all aqueous solutions and for rinsing. Before use, all the glassware was cleaned with freshly prepared aqua regia (HNO_3: HCl) 1:3, % v/v), rinsed thoroughly with water, and dried.

Synthesis of FeCo Nanoparticles. Bimetallic FeCo nanoparticles were synthesized by a procedure described previously for Fe-Ni nanoparticles [31] with some modification. 20 mL of 0.05 M aqueous mixture of $FeSO_4.7H_2O$ and $CoCl_2.6H_2O$ in a Fe:Co atomic ratio of 3:2 was stirred, under nitrogen saturation, for 20 min followed by dropwise addition of 0.6 g $NaBH_4$. The solution colour changed from brownish pink to black upon addition of $NaBH_4$. After further stirring for 20 min, 2 mL of 1 M triethylamine was added to stabilize the nanoparticles. Stirring was continued for an additional 20 min and followed by vacuum filtration through 0.2 μm cellulose acetate filter paper. To get rid of the excess borohydride, the particles were washed with copious amounts of water and rinsed with ethanol and acetone. The washed particles were vacuum dried overnight at 50 ºC.

Characterization

Transmission Electron Microscopy (TEM). The TEM images were recorded using a Tecnai G2 F20X-Twin MAT 200 kV Field Emission Transmission Electron Microscope from FEI (Eindhoven, Netherlands). Samples were prepared by casting a drop of the ethanol-dispersed FeCo nanoparticles over standard carbon-coated copper grids and allowed to dry for analysis. Energy Dispersive X-ray Spectroscopy (EDX) elemental analysis was determined from an EDAX system coupled to the Tecnai G2 TEM machine.

Scanning Electron Microscopy (SEM). The SEM image of the film was captured using Gemini LEO 1525 model microscope.

Electrode Preparation. Bare GCE of area 0.071 cm^2 (diameter, 3mm) or FeCo nanoparticles modified GCE (GCE/FeCo) was used as the working electrode. Platinum wire and Ag/AgCl (3M NaCl) electrodes were used as auxiliary and reference electrodes, respectively. Before every new experiment, the GCE was polished consecutively with alumina slurry (particle sizes- 1.0, 0.3 and 0.05 μm) on a microcloth pad, rinsed and sonicated for 5 min in water. The GCE electrode was modified by drop-coating 5 μL aqueous dispersion of FeCo nanoparticles. The modified electrode was dried and gently rinsed before use.

Voltammetry. Cyclic and square wave voltammograms were recorded with the BAS 100W electrochemical work station from Bio Analytical Systems (Lafayette, USA) in 1 M $LiClO_4$ containing 1:1 v/v EC-DC.

Electrochemical Impedance Spectroscopy (EIS). Impedance measurements were carried out with Zahner IM6ex Germany in 1 M $LiClO_4$ containing 1:1 v/v EC-DC. Alternating current (ac) amplitude of 10 mV within the frequency range of 100 mHz – 100 kHz was used.

Electrocatalytic Oxygen Reduction Reaction (ORR). ORR experiments were conducted in oxygen saturated 1 M $LiClO_4$ containing 1:1 v/v EC-DC electrolyte system using BAS 100W electrochemical work station. Hydrodynamic measurements were obtained from a glassy carbon rotating disc electrode.

Results and Discussion

Characterization of FeCo Nanoparticles. TEM micrographs of the synthesized FeCo nanoparticles as shown in Fig. 1, gave spherical nanoparticles of 35-50 nm in diameter. The nanoparticles are connected in chains of beads due to the magnetic and electronic interaction between the metal particles [32]. Similar TEM images have been reported for FeCo nanoparticles [33-34]. The elemental analysis from EDX as depicted in Table 1 showed that the nanoparticles contain 56.84% Fe and 43.15 % Co. This distribution is close to the original ratio (3:2) of the metal precursors in the reaction mixture. The oxygen peak in the EDX profile as shown in Fig. 2 was due to surface oxidation of FeCo nanoparticles during sample preparation and characterization; the peaks from carbon and copper were from the carbon-coated copper grid used during analysis.

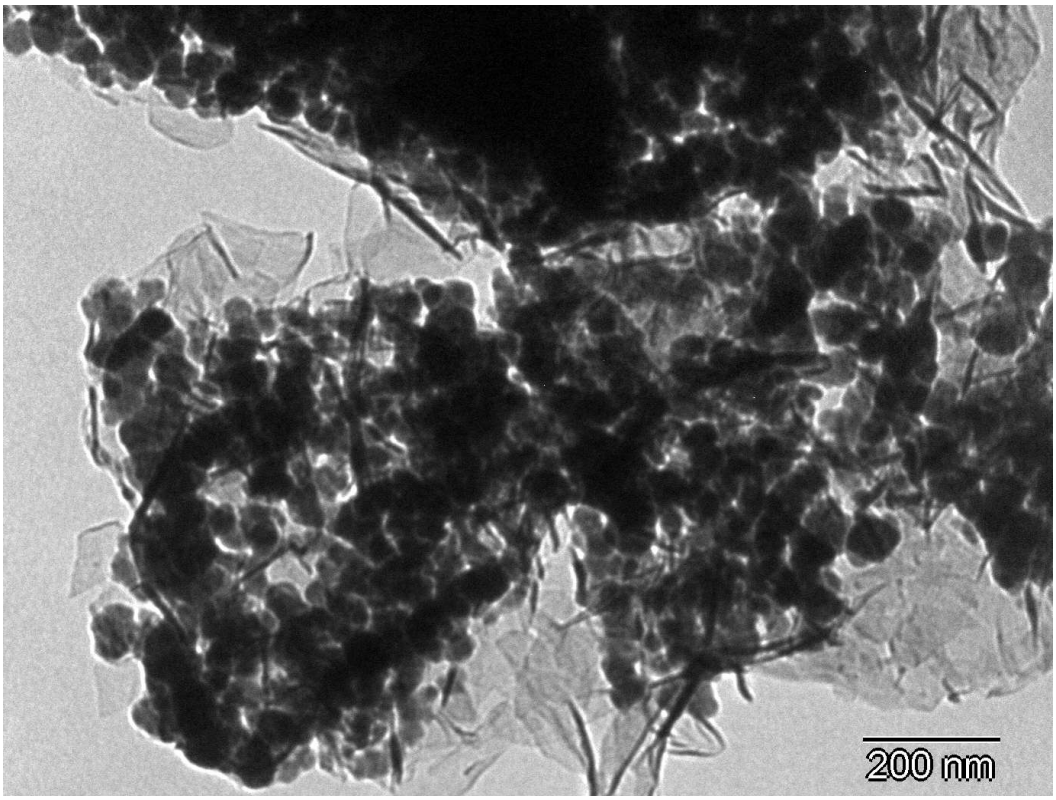

Fig. 1. TEM micrograph of FeCo nanoparticles.

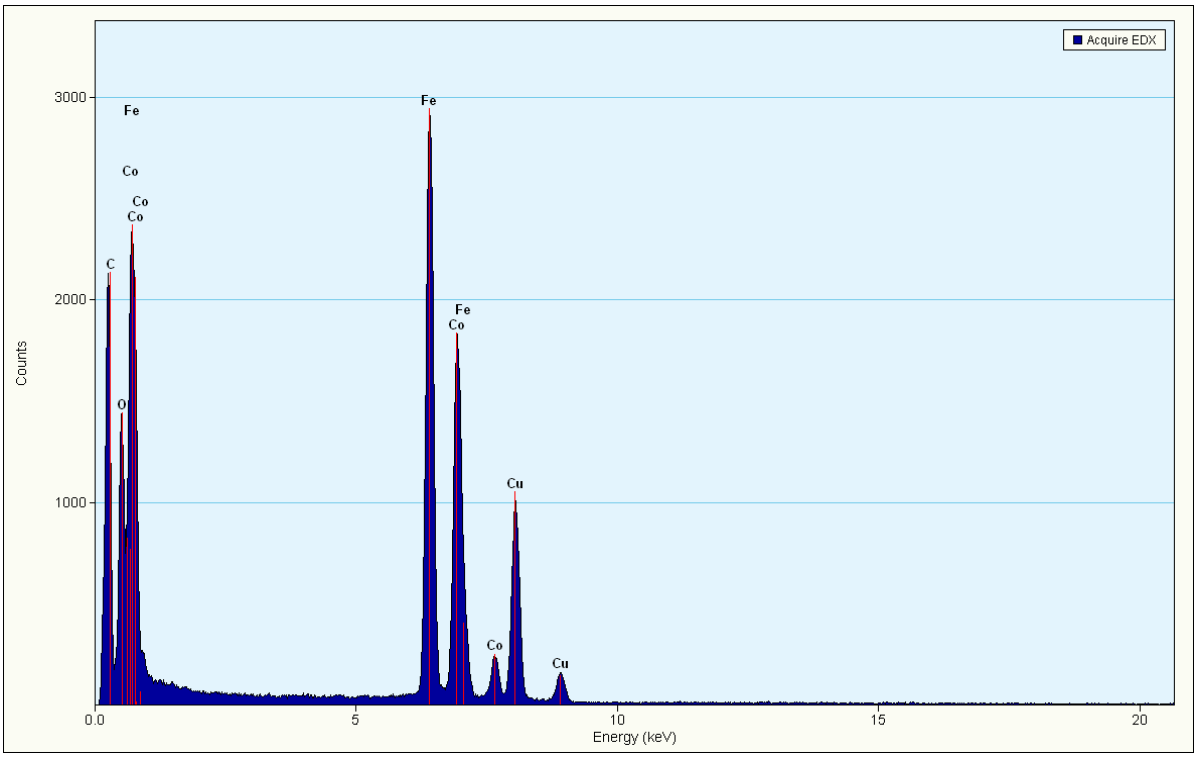

Fig. 2. EDX profile of FeCo nanoparticles.

Table 1. EDX analysis of FeCo nanoparticles.

Element	Weight %	Atomic %	Uncert %	Detector Correction	k-Factor
Fe(K)	56.84	58.16	0.19	0.99	1.403
Co(K)	43.15	41.83	0.16	0.99	1.495

The SEM image in Fig. 3 revealed porous nanoclusters. The porosity will create a large surface area for immobilization of any dopant; also the fact that migration of solvated ionic species depends on the pore size of the film [35], the porosity will greatly enhance the electrochemical and electrocatalytic behaviour of FeCo nanoparticles modified electrodes.

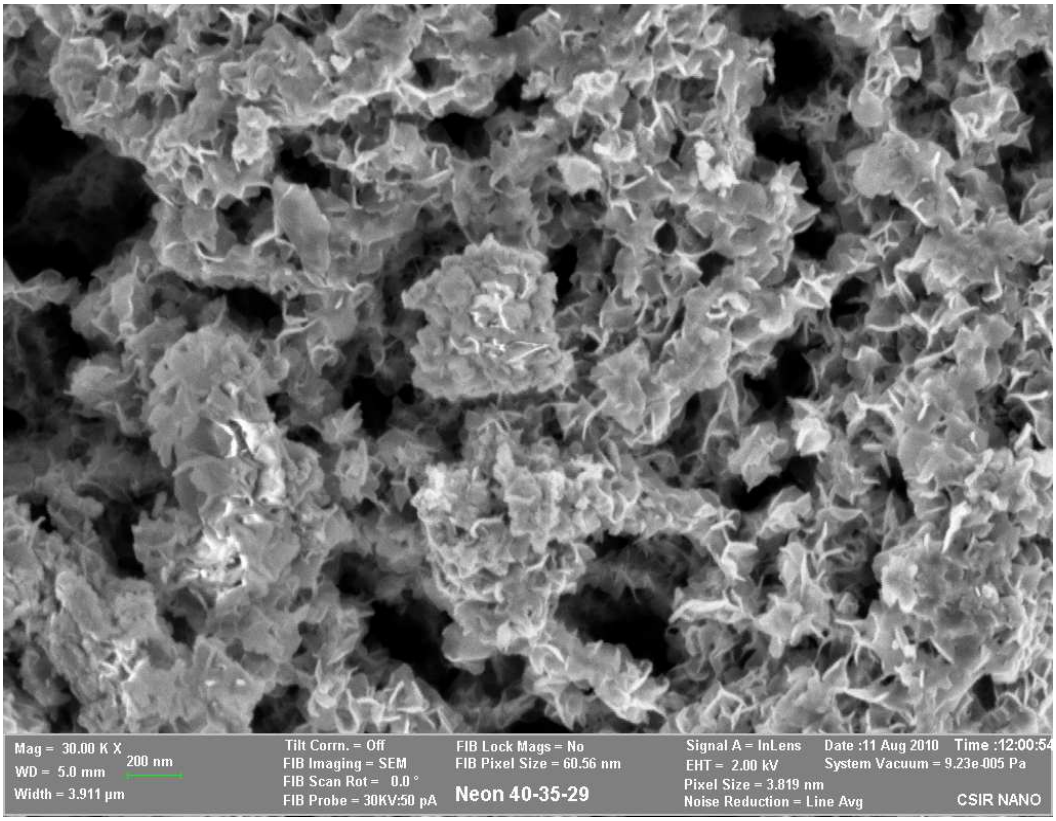

Fig. 3. SEM image of FeCo nanoparticles.

Voltammetric Studies of the FeCo Nanoparticles Modified Glassy Carbon Electrode. Fig. 4(A) shows the cyclic voltammograms (CV) of (i) bare GCE and (ii) GCE/FeCo within a potential window of -800 to 800 mV. As expected, the bare GCE did not exhibit any electrochemistry since there was nothing immobilized on the electrode surface. However, the GCE/FeCo gave an anodic peak, *a*, (I_{pa} = 1.082 µA, E_{pa} = 175 mV) and a cathodic peak, *b*, (I_{pc} = 0.612 µA, E_{pc} = 78 mV) at a formal potential, $\Delta E^{0'}$ = 127 mV. The peak to peak separation, ΔE_p, and the ratio of peak currents, I_{pa}/I_{pc}, were calculated to be 97 mV and 1.77 µA, respectively. Although these were found to be slightly above the values for ideal Nernstian behaviour, they are well within the range of experimentally observed values for a reversible electron transfer process [36-37] and also the fact that electrochemical processes depend on the supporting electrolyte and nature of the film.

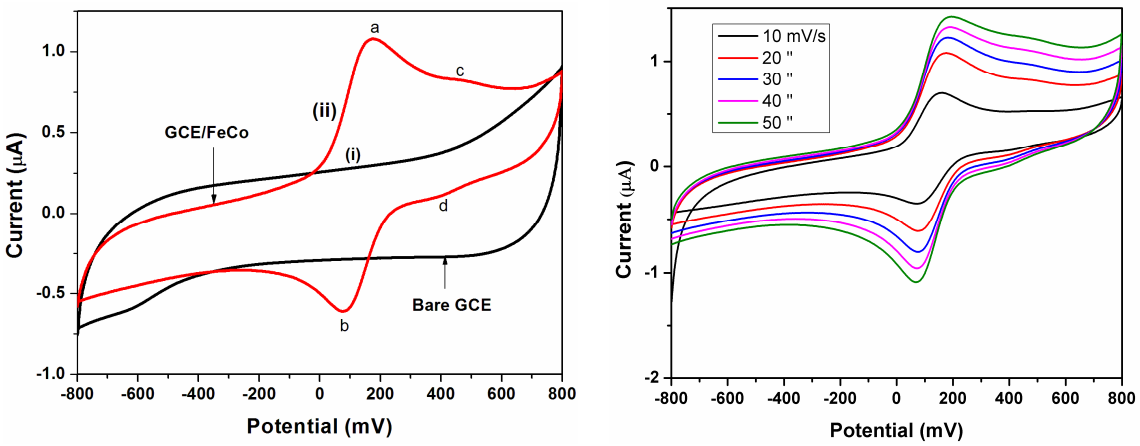

(A) (B)

Fig. 4. Cyclic voltammograms of (A) (i) bare GCE (ii) GCE/FeCo (B) GCE/FeCo at 10, 20, 30, 40 and 50 mV s^{-1} in 1 M $LiClO_4$ electrolyte solution containing 1:1 v/v EC-DC at 25 ºC.

The well defined redox couple can be ascribed to electron transfer reaction of the metal-centered surface-confined redox species Fe^{2+}/Fe^{3+} in the electroactive nanomaterial. A closer evaluation of the CV revealed a diminished redox couple at positions *c*, (I_{pa} = 0.826 µA, E_{pa} = 464 mV) and *d*, (I_{pc} = 0.103 µA, E_{pc} = 387 mV) that is more pronounced in the square wave voltammogram (Fig 5B). The peaks can be attributed to Co^{2+}/Co^{3+} redox transitions on the electrode surface [14]. Fig. 5 shows the square wave voltammograms of (A) bare GCE and (B) GCE/FeCo. The bare electrode gave no discernible electrochemistry while the GCE/FeCo showed two peaks at positions *a*' and *b*'. Peak *a*' corresponds to the oxidation peak, *a*, of the well defined redox couple in the CV while peak *b*' corresponds to the oxidation peak, *c*, of the diminished redox couple in the CV. Scan rate studies showed that the anodic and cathodic peak currents (Fig. 5(C-D)) vary with scan rate. This indicates that the FeCo nanoparticles are electroactive and the diffusion of electrons takes place through the metal cavity as observed from the SEM micrograph. The Randles Sevčik plots in Fig. 5(D) show the linear dependence of peak currents on the square root of scan rates. The non-zero intercepts were due to the contributions of non-Faradaic currents while the linearity confirmed a diffusion-controlled electron transfer process on the electrode/electrolyte interface. The diffusion coefficient, *D*, calculated using equation (1b), gave 4.76 x 10^{-14} cm^2 s^{-1} where *n* (1) is the number of electrons

transferred, A (0.071 cm^2) is the area of the electrode, C (1 x 10^{-3} mol cm^{-3}) is the concentration of the bulk electrolyte solution and $I_p/v^{1/2}$ (4.16617 x 10^{-6}A $s^{1/2}$ $V^{-1/2}$) is the slope of the I_p versus $v^{1/2}$ linear plot (anodic plot of Fig. 5 (D)). The value of D was affected by the concentration of the electrolyte used in this study and is generally subject to uncertainties in volume and homogeneity of the film [38-39].

$$I_p = (2.69 \times 10^5)\, n^{3/2} A D^{1/2} C v^{1/2} \quad (1a)$$

$$I_p/v^{1/2} = (2.69 \times 10^5)\, n^{3/2} A D^{1/2} C \quad (1b)$$

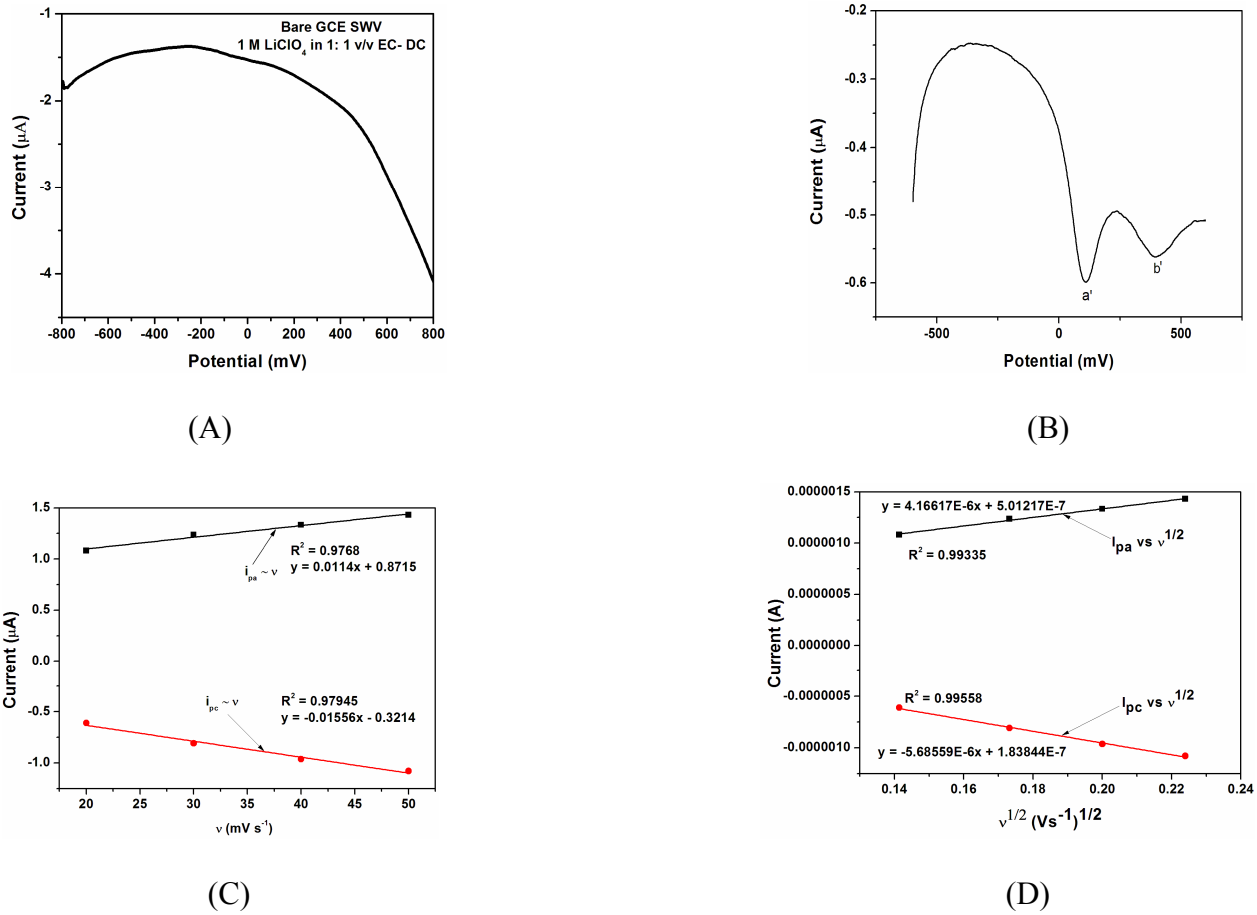

Fig. 5. (A-B) Square wave voltammogram of (A) bare GCE (B) GCE/FeCo; (C-D) the plots of the dependence of the peak currents (C) on scan rates (D) as a function of the square root of scan rates.

Further investigation from the plot of peak potentials versus scan rates (Fig. 6A) revealed the dependence of peak potentials on scan rates. While the E_{pa} was seen to increase, E_{pc} decreases as scan rate increases.

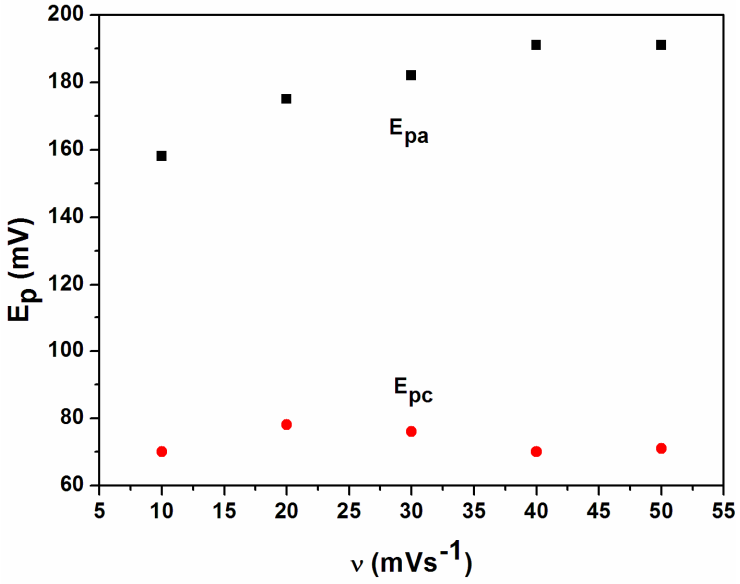

Fig. 6. The plot of the dependence of the peak potentials versus scan rates.

The surface concentration (Γ) of the FeCo film on GCE was obtained from the integrated charges of the anodic CV curve in accordance with the equation for ideal, reversible thin layer electrochemistry [40]:

$$I_p = n^2F^2A\Gamma\, v/4RT \quad (2)$$

$$Q = nFA\Gamma \quad (3)$$

where F = Faraday constant (96485 C mol^{-1}), v = scan rate, R = gas constant (8.314 J mol^{-1}K^{-1}), T = absolute temperature (298 K), other parameters have their usual meanings. The voltammetric behaviour of the FeCo modified GCE within the scan rate range of 10 - 50 mV s^{-1} showed that the calculated Γ at 10 mV s^{-1} gave the best surface coverage with a value of 5 x 10^{-9} mol cm^{-2}. In

addition, the fact that a lower peak to peak separation (ΔE_p) value was recorded at this scan rate showed that the FeCo modified electrode exhibited a faster electron transfer at lower scan rates. The Γ value is well within the range of values reported previously [39, 41].

EIS Studies. EIS was used to investigate the interfacial properties of the bare and GCE/FeCo electrodes. This was conducted by recording the impedance spectra of the electrodes in $LiClO_4$ supporting electrolyte. Each Nyquist plot (Fig. 7 (A)) showed a semi-circle and a Warburg diffusion line which is an indication that the electrochemical process on the electrode surface is kinetically controlled at higher frequencies and diffusion controlled at lower frequencies. The inset equivalent circuit was developed to fit the impedance parameters. R_s is the resistance of the electrolyte solution which was obtained from the intercept of the semi-circle with the Z' axis at higher frequencies; the diameter of the semi-circle is related to the charge transfer resistance, R_{ct}, which controls the transfer kinetics at the electrode interface. Extrapolation of the semi-circle to lower frequencies gave an intercept corresponding to $R_s + R_{ct}$ from which the value of R_{ct} was determined; Z_w is the Warburg impedance which measures the mass transport of materials occurring through a diffusion-controlled process; CPE is the constant phase element that models the double layer capacitance (C_{dl}) which is due to surface roughness.

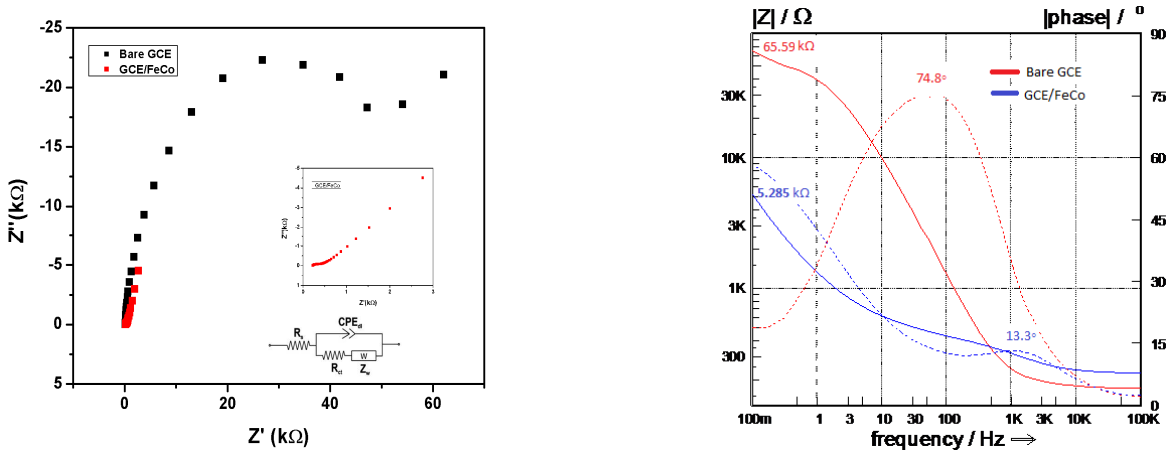

(A) (B)

Fig. 7. (A) Nyquist and (B) Bode plots of bare GCE and GCE/FeCo.

Analytically meaningful impedance spectra are usually recorded at higher frequencies where they are mainly controlled by the interfacial properties of the modified electrodes [42]. The bare electrode exhibited a wider semicircle at higher frequency with an R_{ct} value of 44.12 kΩ which is two orders of magnitude higher than the R_{ct} value of 159 Ω obtained for the GCE/FeCo electrode. This decrease is attributed to the presence of electroactive FeCo nanoparticles which promote the rate of electron transfer and therefore suggests a higher conductivity on the nanoelectrode than on the bare GCE. Similar trends were observed in the values of the exchange current (i_o) and rate constant of electron transfer (k_{et}) as shown in Table 2. This phenomenon is corroborated by the Bode plots (Fig. 7 (B)) where the impedance decreased from 65.59 kΩ (for the bare GCE) to 5.285 kΩ (for the GCE/FeCo) at lower frequency regimes where disturbances to the equilibrium positions of the systems are minimal. A corresponding decrease in phase angle from 74.8° to 13.3° was observed which further confirmed the higher conducting properties of the nanoelectrode over the bare GCE. Time constant (τ), i_o and k_{et} were calculated according to equations, 4 – 7 [40, 43-45]:

$$\omega_{max} = 2\pi f_{max} = \frac{1}{R_{ct}C_{dl}} \tag{4}$$

$$\tau = \frac{1}{\omega_{max}} = R_{ct}C_{dl} \tag{5}$$

$$R_{ct} = \frac{RT}{nFi_o} \tag{6}$$

$$i_o = nFAk_{et}C \tag{7}$$

The values obtained for the kinetic parameters also revealed an improved electrochemical performance of the nanoelectrode over the bare GCE as illustrated in Table 2.

Table 2. Kinetic data from EIS

Nature of electrode	**ω (rad s^{-1})**	**τ (s rad^{-1})**	**i_o (A cm^{-2})**	**k_{et} (cm s^{-1})**
Bare GCE	9.01	1.1 x 10^{-1}	5.82 x 10^{-7}	8.4 x 10^{-8}
GCE/FeCo	4159.0	2.4 x 10^{-4}	1.6 x 10^{-4}	2.3 x 10^{-5}

Electrocatalytic Oxygen Reduction Reaction. The electrochemical response of the FeCo modified GCE towards oxygen reduction was investigated by cyclic voltammetric and hydrodynamic techniques in 1 M $LiClO_4$ containing 1:1 v/v EC-DC. Fig. 8A shows the cyclic voltammograms of the bare and GCE/FeCo electrodes in the presence and absence of oxygen within a potential range of 200 to -1500 mV. The oxygen reduction process occurred irreversibly with an enhancement in the cathodic peak current of the nanoelectrode in the presence of oxygen when compared with the bare and GCE/FeCo electrodes in the absence of oxygen. However, the onset potential of oxygen reduction on the modified electrode is about 87 mV later than that of the bare electrode. Fig. 8B shows the cyclic voltammograms of the GCE/FeCo electrode saturated with oxygen at various scan rates. A linear correlation (Fig. 9A) between the cathodic current and $\nu^{1/2}$ suggests that the kinetics of the overall process are controlled by mass transport of molecular oxygen (O_2) from the bulk solution to the electrode surface. The cathodic peaks shifted to more negative potential values with increasing ν. A kinetic limitation therefore exists in the ORR process at higher scan rates. This phenomenon has been previously reported [46]. The oxygen reduction process is governed by equations 8 - 9 [40, 47]:

$$E_p = \frac{b}{2}\log \nu \tag{8}$$

$$b = \frac{2.303RT}{\alpha nF} \tag{9}$$

where b is the Tafel slope, α is the charge transfer coefficient, other parameters have their usual meanings. From the linear plot of E_p versus $\log \nu$ (Fig. 9B), a Tafel slope of approximately 120 mV and α value of 0.49 were obtained. The Tafel slope is close to the theoretical 118 mV for a one electron process [40] involved in the rate determining step. These values are in good agreement with previously reported experimental results [48].

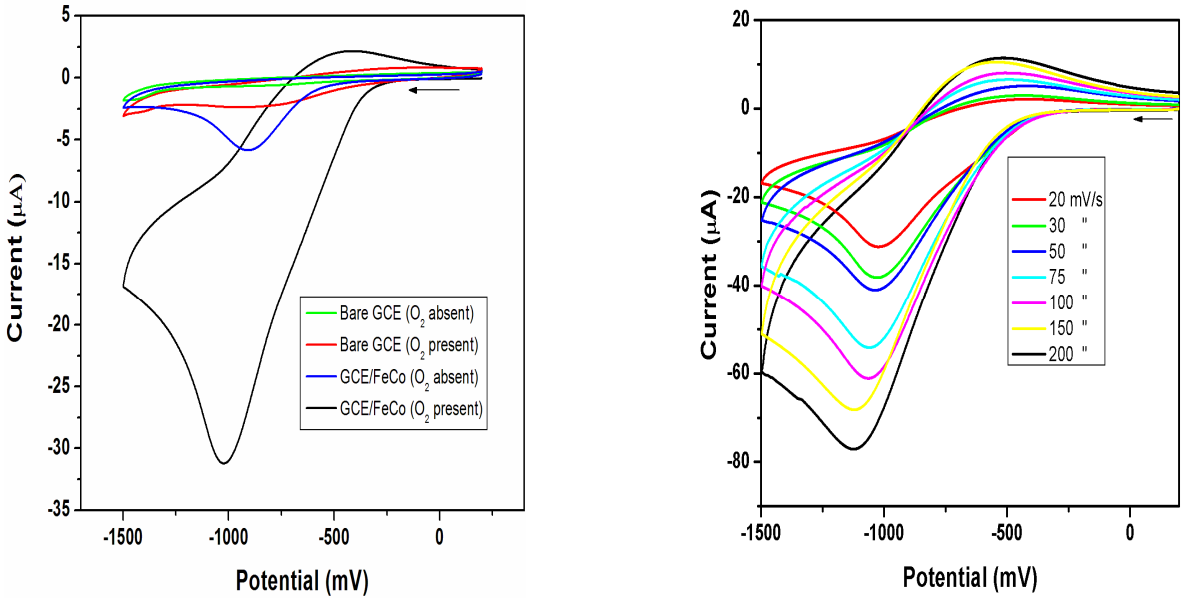

A B

Fig. 8. (A) Cyclic voltammograms of the modified and unmodified GCE in 1 M $LiClO_4$ containing 1:1 v/v EC-DC at a scan rate of 20 mV s^{-1} in the absence and presence of saturated oxygen between 200 to -1500 mV (B) Cyclic voltammograms of the modified GCE in oxygen saturated 1 M $LiClO_4$ containing 1:1 v/v EC-DC at various scan rates.

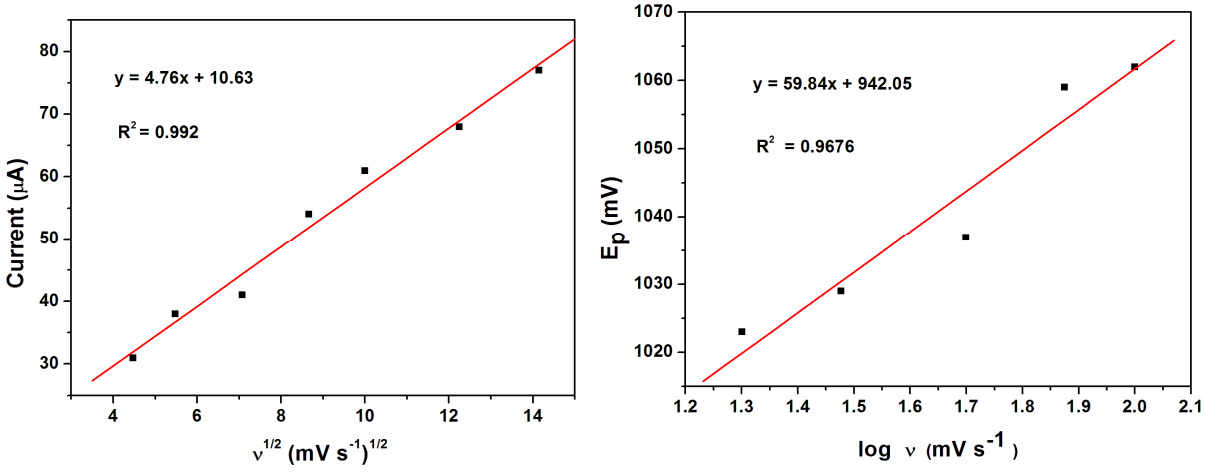

A B

Fig. 9. (A) Plot of current (I_{pc}) versus $\nu^{1/2}$. (B) Tafel plot of E_p versus logν.

Hydrodynamic voltammetry with rotating disc electrode (RDE) was qualitatively used to study the electrochemical catalytic reduction of molecular oxygen at GCE/FeCo electrode by recording the linear scans of the RDE voltammograms from -300 to -1500 mV in oxygen saturated 1 M $LiClO_4$ containing 1:1 v/v EC-DC. Fig.10A showed that the current increased with increasing rotation rate. The Koutecky-Levich plot for the electro-catalytic reduction of molecular oxygen on GCE/FeCo in oxygen saturated 1 M $LiClO_4$ containing 1:1 v/v EC-DC is shown in Fig. 10B. It is well known that O_2 is electrochemically reduced to super-oxide ion (O_2^-) in non-aqueous aprotic media [49-50]. However, the mechanism of this reduction in the electrolyte under study could not be established at this stage.

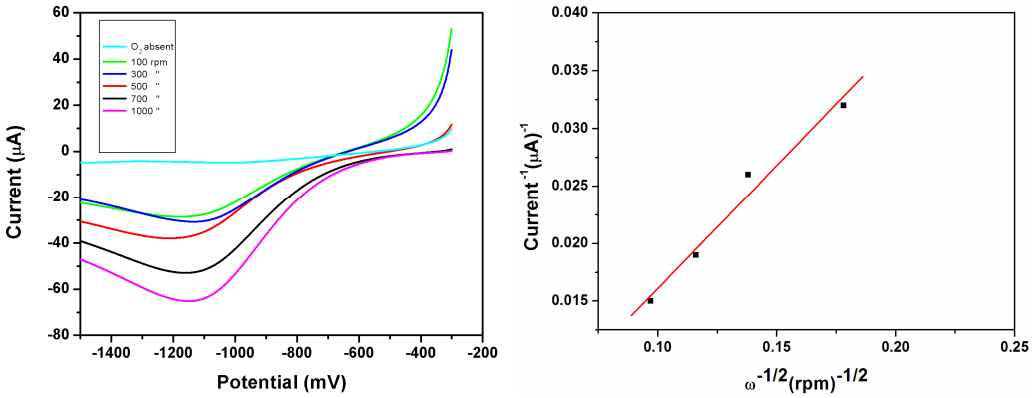

A B

Fig. 10. (A) Current-potential plot for oxygen reduction on GCE/FeCo in the absence of oxygen at a rotation rate of 100 rpm and at different rotation rates in an oxygen saturated solution. (B) Kouteky-Levich plot for oxygen reduction.

Conclusion

This study reveals for the first time, the electrochemical dynamics of FeCo nanoparticles - modified glassy carbon electrode in 1 M $LiClO_4$ containing 1:1 v/v ethylene carbonate-dimethyl carbonate electrolyte system by employing cyclic and square wave voltammetric techniques as well as electrochemical impedance spectroscopy. The nanoelectrode showed enhanced electroactivity over the unmodified glassy carbon electrode and good response towards electrocatalytic reduction of molecular oxygen.

Acknowledgment

NRF and CSIR are gratefully acknowledged.

References

[1] J.J. Gooding, L.M.H. Lai, I. Y. Goon, Nanostructured electrodes with unique properties for biological and other applications, in: R.C. Alkire, D.M. Kolb, J. Lipkowski, P.N. Ross, (Eds.), Chemically Modified Electrodes, WILEY-VCH Verlag GmbH & Co. KGaA, Weinheim Germany, 2009, pp. 1 - 56.

[2] N.M. Markovic, P.N. Ross, Surface science studies of model fuel cell electrocatalysts, Surf. Sci. Rep. 45 (2002) 117-229.

[3] J. Mathiyarasu, S.S. Pathak, V. Yegnaraman, Review on corrosion prevention of copper using ultrathin organic monolayers, Corros. Rev. 24 (2006) 307-321.

[4] G. Ybarra, C. Moina, M.I. Florit, D. Posadas, Current rectification by mediating electroactive polymers, Electrochim. Acta. 53 (2008) 3955-3959.

[5] R. J. Mortimer, Electrochromic materials, Chem. Soc. Rev. 26 (1997) 147-156.

[6] R. A. Durst, A. J. Baumner, R.W. Murray, R.P. Buck, C.P. Andrieux, Chemically modified electrodes: recommended terminology and definitions, Pure Appl. Chem. 69 (1997) 1317-1323.

[7] R. Gulaboski, M. Chirea, C.M. Pereira, M.N.D.S. Cordeiro, R.B. Costa, A.F. Silva, Probing of the voltammetric features of graphite electrodes modified with mercaptoundecanoic acid stabilized gold nanoparticles, J. Phys. Chem. C. 112 (2008) 2428-2435.

[8] M.M. Ardakani, A. Talebi, H. Naeimi, M.N. Barzoky, N. Taghavinia, Fabrication of modified TiO_2 nanoparticle carbon paste electrode for simultaneous determination of dopamine, uric acid, and l-cysteine, J. Solid State Electrochem. 13 (2009) 1433-1440.

[9] R.P. Kingsborough, T.M. Swager, Electrocatalytic conducting polymers: oxygen reduction by a polythiophene−cobalt salen hybrid, Chem. Mater. 12 (2000) 872-874.

[10] L.S.M. Santos, J. Ghilane, C. Fave, P.-C. Lacaze, H. Randriamahazaka, L.M. Abrantes, J.-C. Lacroix, Electrografting polyaniline on carbon through the electroreduction of diazonium salts and the electrochemical polymerization of aniline, J. Phys. Chem. C. 112 (2008) 16103-16109.

[11] H. Luo, Z. Shi, N. Li, Z. Gu, Q. Zhuang, Investigation of the electrochemical and electrocatalytic behavior of single-wall carbon nanotube film on a glassy carbon electrode, Anal. Chem. 73 (2001) 915-920.

[12] S. Yang, L. Qu, G. Li, R. Yang, C. Liu, Gold nanoparticles/ethylenediamine/carbon nanotube modified glassy carbon electrode as the voltammetric sensor for selective determination of rutin in the presence of ascorbic acid, J. Electroanal. Chem. 645 (2010) 115-122.

[13] C. Fu, Y. Kuang, Z. Huang, X. Wanga, N. Du, J. Chen, H. Zhou, Electrochemical co-reduction synthesis of graphene/Au nanocomposites in ionic liquid and their electrochemical activity, Chem. Phys. Lett. 499 (2010) 250-253.

[14] M. Tabeshnia, M. Rashvandavei, R. Amini, F. Pashaee, Electrocatalytic oxidation of some amino acids on a cobalt hydroxide nanoparticles modified glassy carbon electrode, J. Electroanal. Chem. 647 (2010) 181-186.

[15] R. Nagarajan, T.A. Hatton, Nanoparticles: Synthesis, Stabilization, Passivation, and Functionalization. American Chemical Soc., Washington DC, 2008.

[16] J. Rodriguez, Physical and chemical properties of bimetallic surfaces, Surf. Sci. Rep. 24 (1996) 223-287.

[17] J. Zhang, J.-O. Müller, W. Zheng, D. Wang, D. Su, R. Schlögl, Individual Fe−Co alloy nanoparticles on carbon nanotubes: structural and catalytic properties, Nano Lett. 8 (2008) 2738-2743.

[18] H. Moumeni, S. Alleg, J.M. Greneche, Structural properties of $Fe_{50}Co_{50}$ nanostructured powder prepared by mechanical alloying, J. Alloys Compd. 386 (2005) 12-19.

[19] M. Sorescu, A. Grabias, Structural and magnetic properties of $Fe_{50}co_{50}$ system, Intermetallics. 10 (2002) 317-321.

[20] A. Zelenáková, D. Oleksáková, J. Degmová, J. Kovác, P. Kollár, M. Kusý, P. Sovák, Structural and Magnetic Properties of Mechanically Alloyed Feco Powders, J. Magn. Magn. Mater. 316 (2007) e519-e522.

[21] K.J. Kim, S.J. Lee, D.W. Lynch, Study of optical properties and electronic structure of ferromagnetic FeCo, Solid State Commun. 114 (2000) 457-460.

[22] P.-S. Yuan, H.-Q. Wu, H.-Y. Xu, D.-M. Xu, Y.-J. Cao, X.-W. Wei, Synthesis, characterization and electrocatalytic properties of FeCo alloy nanoparticles supported on carbon nanotubes, Mater. Chem. and Phys. 105 (2007) 391-394.

[23] R. Elkalkouli, M. Grosbras, J.F. Dinhut, Mechanical and magnetic properties of nanocrystalline FeCo alloys produced by mechanical alloying, Nanostruct. Mater. 5 (1995) 733-743.

[24] T. Sourmail, Near equiatomic FeCo alloys: constitution, mechanical and magnetic properties, Prog. Mater. Sci. 50 (2005) 816-880.

[25] C. Jo, J.I. Lee, Y. Jang, Electronic and magnetic properties of ultrathin Fe–Co alloy nanowires, Chem. Mater. 17 (2005) 2667-2671.

[26] R.J. Joseyphus, K. Shinoda, D. Kodama, B. Jeyadevan, Size controlled Fe nanoparticles through polyol process and their magnetic properties, Mater. Chem. Phys. 123 (2010) 487-493.

[27] M. Yamada, S.-J. Okumura, K. Takahashi, Synthesis and film formation of magnetic FeCo nanoparticles with graphitic carbon shells, J. Phys. Chem. Lett. 1 (2010) 2042-2045.

[28] G.S. Chaubey, C. Barcena, N. Poudyal, C. Rong, J. Gao, S. Sun, J.P. Liu, Synthesis and stabilization of FeCo nanoparticles, J. Am. Chem. Soc. 129 (2007) 7214-7215.

[29] C. Wang, R. Lv, F. Kang, J. Gu, X. Gui, D. Wu, Synthesis and application of iron-filled carbon nanotubes coated with FeCo alloy nanoparticles, J. Magn. Magn. Mater. 321 (2009) 1924-1927.

[30] X. Lu, G. Liang, Y. Zhang, Structure and magnetic properties of FeCo-SiO_2 nanocomposite synthesized by a novel wet chemical method, Mater. Lett. 61 (2007) 4928-4931.

[31] A.D. Bokare, R.C. Chikate, C.V. Rode, K.M. Paknikar, Effect of surface chemistry of Fe−Ni nanoparticles on mechanistic pathways of azo dye degradation, Environ. Sci. Technol. 41 (2007) 7437-7443.

[32] M. Hesani, A. Yazdani, B. Abedi Ravan, M. Ghazanfari, The effect of particle size on the characteristics of FeCo nanoparticles, Solid State Commun. 150 (2010) 594-597.

[33] S.K. Pal, D. Bahadur, Shape controlled synthesis of iron–cobalt alloy magnetic nanoparticles using soft template method, Mater. Lett. 64 (2010) 1127-1129.

[34] S.J. Shin, Y.H. Kim, C.W. Kim, H.G. Cha, Y.J. Kim, Y.S. Kang, Preparation of magnetic FeCo nanoparticles by co-precipitation route, Curr. Appl. Phys. **7** (2007) 404-408.

[35] N.F. Atta, M.F. El-Kady, Poly(3-methylthiophene)/palladium sub-micro-modified sensor electrode. Part II: Voltammetric and EIS studies, and analysis of catecholamine neurotransmitters, ascorbic acid and acetaminophen, Talanta 79 (2009) 639-647.

[36] D.K. Gosser, Cyclic Voltammetry: Simulation and Analysis of Reaction Mechanisms. VCH Publishers, Inc. New York, 1993.

[37] X. Li, H. Qi, L. Shen, Q. Gao, C. Zhang, Electrochemical aptasensor for the determination of cocaine incorporating gold nanoparticles modification, Electroanalysis 13 (2008) 1475-1482.

[38] E.I. Iwuoha, D. Saenz de Villaverde, N.P. Garcia, M.R. Smyth, J.M. Pingarron, Reactivities of organic phase biosensors. 2. The amperometric behaviour of horseradish peroxidase immobilised on a platinum electrode modified with an electrosynthetic polyaniline film, Biosens. Bioelectron. 12 (1997) 749-761.

[39] J.F. Rusling, H. Zhang, Multilayer films of cationic surfactants on electrodes. control of charge transport by phase, Langmuir **7** (1991) 1791-1796.

[40] A.J. Bard, L.R. Faulkner, Electrochemical Methods: Fundamentals and Applications, Second ed., John Wiley & Sons, Inc. 2001.

[41] M.M. Ardakani, P.E. Karami, P. Rahimi, H.R. Zare, H. Naeimi, Electrocatalytic hydrazine oxidation on quinizarine modified glassy carbon electrode, Electrochim. Acta. 52 (2007) 6118-6124.

[42] E. Katz, I. Willner, Probing biomolecular interactions at conductive and semiconductive surfaces by impedance spectroscopy: routes to impedimetric immunosensors, DNA-sensors, and enzyme biosensors, Electroanalysis 15 (2003) 913-947.

[43] S.-M. Park, J.-S. Yoo, Peer Reviewed: Electrochemical impedance spectroscopy for better electrochemical measurements, Anal. Chem. 75 (2003) 455 A - 461 A.

[44] R. Greef, R. Peat, L.M. Peter, D. Pletcher, J. Robinson, Instrumental Methods in Electrochemistry. Ellis Horwood, 1990.

[45] F. Sundfors, J. Bobacka, A. Ivaska, A. Lewenstam, kinetics of electron transfer between $Fe(CN)_6^{3-/4-}$ and poly(3,4-ethylenedioxythiophene) studied by electrochemical impedance spectroscopy, Electrochim. Acta. 47 (2002) 2245-2251.

[46] M. Shamsipur, M. Najafi, M.-R. M. Hosseini, H. Sharghi, Electrocatalytic reduction of dioxygen at carbon paste electrode modified with a novel cobalt(III) Schiff"S base complex, Electroanalysis 19 (2007) 1661-1667.

[47] J.A. Harrison, Z.A. Khan, The Oxidation of Hydrazine on Platinum in Acid Solution, J. Electroanal. Chem. Interfacial Electrochem. 28 (1970) 131-138.

[48] S.A. Mamuru, K.I. Ozoemena, T. Fukuda, N. Kobayashi, T. Nyokong, Studies on the heterogeneous electron transport and oxygen reduction reaction at metal (Co, Fe) octabutylsulphonylphthalocyanines supported on multi-walled carbon nanotube modified graphite electrode, Electrochim. Acta 55 (2010) 6367-6375.

[49] C.O. Laoire, S. Mukerjee, K.M. Abraham, E.J. Plichta, M.A. Hendrickson, Influence of nonaqueous solvents on the electrochemistry of oxygen in the rechargeable lithium−air battery, J. Phys. Chem. C. 114 (2010) 9178-9186.

[50] M. Tsushima, K. Tokuda, T. Ohsaka, Use of hydrodynamic chronocoulometry for simultaneous determination of diffusion coefficients and concentrations of dioxygen in various media, Anal Chem. **66** (1994) 4551-4556.